Space-division multiplexing optical coherence tomography

Chao Zhou,[1,2,3,*] Aneesh Alex,[1,2] Janarthanan Rasakanthan,[1,2] and Yutao Ma[1,2,4]

[1]*Department of Electrical and Computer Engineering, Lehigh University, Bethlehem, Pennsylvania 18015, USA*
[2]*Center for Photonics and Nanoelectronics, Lehigh University, Bethlehem, Pennsylvania 18015, USA*
[3]*Bioengineering Program, Lehigh University, Bethlehem, Pennsylvania 18015, USA*
[4]*State Key Lab of Software Engineering, Wuhan University, Wuhan, 430072, China*
[*]*chaozhou@lehigh.edu*

Abstract: High speed, high resolution and high sensitivity are desirable for optical coherence tomography (OCT). Here, we demonstrate a space-division multiplexing (SDM) technology that translates long coherence length of a commercially available wavelength tunable laser into high OCT imaging speed. We achieved an effective 800,000 A-scans/s imaging speed using a 100,000 Hz tunable vertical cavity surface-emitting laser (VCSEL). A sensitivity of 94.6 dB and a roll-off of < 2 dB over ~30 mm imaging depth were measured from a single channel in the prototype SDM-OCT system. An axial resolution of ~11 μm in air (or ~8.3 μm in tissue) was achieved throughout the entire depth range. An *in vivo*, 3D SDM-OCT volume of an entire *Drosophila* larva consisting of 400 x 605 A-scans was acquired in 0.37 seconds. Synchronized cross-sectional OCT imaging of three different segments of a beating *Drosophila* larva heart is demonstrated. The SDM technology provides a new orthogonal dimension for further speed improvement for OCT with favorable cost scaling. SDM-OCT also preserves image resolution and allows synchronized cross-sectional and three-dimensional (3D) imaging of biological samples, enabling new biomedical applications.

OCIS codes: (110.4500) Optical coherence tomography; (060.4230) Multiplexing; (110.6880) Three-dimensional image acquisition; (170.3880) Medical and biological imaging.

References and links

1. D. Huang, E. A. Swanson, C. P. Lin, J. S. Schuman, W. G. Stinson, W. Chang, M. R. Hee, T. Flotte, K. Gregory, C. A. Puliafito, and J. G. Fujimoto, "Optical coherence tomography," Science **254**(5035), 1178–1181 (1991).
2. W. Drexler, U. Morgner, R. K. Ghanta, F. X. Kärtner, J. S. Schuman, and J. G. Fujimoto, "Ultrahigh-resolution ophthalmic optical coherence tomography," Nat. Med. **7**(4), 502–507 (2001).
3. J. G. Fujimoto, "Optical coherence tomography for ultrahigh resolution in vivo imaging," Nat. Biotechnol. **21**(11), 1361–1367 (2003).
4. B. Potsaid, I. Gorczynska, V. J. Srinivasan, Y. L. Chen, J. Jiang, A. Cable, and J. G. Fujimoto, "Ultrahigh speed Spectral / Fourier domain OCT ophthalmic imaging at 70,000 to 312,500 axial scans per second," Opt. Express **16**(19), 15149–15169 (2008).
5. L. An, P. Li, T. T. Shen, and R. K. Wang, "High speed spectral domain optical coherence tomography for retinal imaging at 500,000 A-lines per second," Biomed. Opt. Express **2**(10), 2770–2783 (2011).
6. T. Schmoll and R. A. Leitgeb, "Heart-beat-phase-coherent Doppler optical coherence tomography for measuring pulsatile ocular blood flow," J Biophotonics **6**(3), 275–282 (2013).
7. W. Wieser, B. R. Biedermann, T. Klein, C. M. Eigenwillig, and R. Huber, "Multi-megahertz OCT: high quality 3D imaging at 20 million A-scans and 4.5 GVoxels per second," Opt. Express **18**(14), 14685–14704 (2010).
8. R. Huber, M. Wojtkowski, and J. G. Fujimoto, "Fourier Domain Mode Locking (FDML): A new laser operating regime and applications for optical coherence tomography," Opt. Express **14**(8), 3225–3237 (2006).
9. R. Huber, D. C. Adler, and J. G. Fujimoto, "Buffered Fourier domain mode locking: unidirectional swept laser sources for optical coherence tomography imaging at 370,000 lines/s," Opt. Lett. **31**(20), 2975–2977 (2006).
10. M. A. Choma, M. V. Sarunic, C. H. Yang, and J. A. Izatt, "Sensitivity advantage of swept source and Fourier domain optical coherence tomography," Opt. Express **11**(18), 2183–2189 (2003).
11. J. F. de Boer, B. Cense, B. H. Park, M. C. Pierce, G. J. Tearney, and B. E. Bouma, "Improved signal-to-noise ratio in spectral-domain compared with time-domain optical coherence tomography," Opt. Lett. **28**(21), 2067–2069 (2003).

#192229 - $15.00 USD Received 14 Jun 2013; revised 15 Jul 2013; accepted 31 Jul 2013; published 6 Aug 2013

12. R. Leitgeb, C. K. Hitzenberger, and A. F. Fercher, "Performance of fourier domain vs. time domain optical coherence tomography," Opt. Express **11**(8), 889–894 (2003).
13. B. Potsaid, B. Baumann, D. Huang, S. Barry, A. E. Cable, J. S. Schuman, J. S. Duker, and J. G. Fujimoto, "Ultrahigh speed 1050nm swept source/Fourier domain OCT retinal and anterior segment imaging at 100,000 to 400,000 axial scans per second," Opt. Express **18**(19), 20029–20048 (2010).
14. S. Zotter, M. Pircher, T. Torzicky, M. Bonesi, E. Götzinger, R. A. Leitgeb, and C. K. Hitzenberger, "Visualization of microvasculature by dual-beam phase-resolved Doppler optical coherence tomography," Opt. Express **19**(2), 1217–1227 (2011).
15. D. Choi, H. Hiro-Oka, H. Furukawa, R. Yoshimura, M. Nakanishi, K. Shimizu, and K. Ohbayashi, "Fourier domain optical coherence tomography using optical demultiplexers imaging at 60,000,000 lines/s," Opt. Lett. **33**(12), 1318–1320 (2008).
16. D. H. Choi, H. Hiro-Oka, K. Shimizu, and K. Ohbayashi, "Spectral domain optical coherence tomography of multi-MHz A-scan rates at 1310 nm range and real-time 4D-display up to 41 volumes/second," Biomed. Opt. Express **3**(12), 3067–3086 (2012).
17. M. Wojtkowski, A. Kowalczyk, R. Leitgeb, and A. F. Fercher, "Full range complex spectral optical coherence tomography technique in eye imaging," Opt. Lett. **27**(16), 1415–1417 (2002).
18. E. Götzinger, M. Pircher, R. Leitgeb, and C. Hitzenberger, "High speed full range complex spectral domain optical coherence tomography," Opt. Express **13**(2), 583–594 (2005).
19. A. M. Davis, M. A. Choma, and J. A. Izatt, "Heterodyne swept-source optical coherence tomography for complete complex conjugate ambiguity removal," J. Biomed. Opt. **10**(6), 064005 (2005).
20. A. H. Bachmann, R. Michaely, T. Lasser, and R. A. Leitgeb, "Dual beam heterodyne Fourier domain optical coherence tomography," Opt. Express **15**(15), 9254–9266 (2007).
21. B. J. Vakoc, S. H. Yun, G. J. Tearney, and B. E. Bouma, "Elimination of depth degeneracy in optical frequency-domain imaging through polarization-based optical demodulation," Opt. Lett. **31**(3), 362–364 (2006).
22. Y. Yasuno, S. Makita, T. Endo, G. Aoki, M. Itoh, and T. Yatagai, "Simultaneous B-M-mode scanning method for real-time full-range Fourier domain optical coherence tomography," Appl. Opt. **45**(8), 1861–1865 (2006).
23. B. Hofer, B. Považay, B. Hermann, A. Unterhuber, G. Matz, and W. Drexler, "Dispersion encoded full range frequency domain optical coherence tomography," Opt. Express **17**(1), 7–24 (2009).
24. A.-H. Dhalla, D. Nankivil, and J. A. Izatt, "Complex conjugate resolved heterodyne swept source optical coherence tomography using coherence revival," Biomed. Opt. Express **3**(3), 633–649 (2012).
25. M. Zurauskas, A. Bradu, and A. G. Podoleanu, "Frequency multiplexed long range swept source optical coherence tomography," Biomed. Opt. Express **4**(6), 778–788 (2013).
26. A. H. Dhalla, D. Nankivil, T. Bustamante, A. Kuo, and J. A. Izatt, "Simultaneous swept source optical coherence tomography of the anterior segment and retina using coherence revival," Opt. Lett. **37**(11), 1883–1885 (2012).
27. M. Yamanari, S. Makita, Y. Lim, and Y. Yasuno, "Full-range polarization-sensitive swept-source optical coherence tomography by simultaneous transversal and spectral modulation," Opt. Express **18**(13), 13964–13980 (2010).
28. C. Fan, Y. Wang, and R. K. Wang, "Spectral domain polarization sensitive optical coherence tomography achieved by single camera detection," Opt. Express **15**(13), 7950–7961 (2007).
29. B. Baumann, W. Choi, B. Potsaid, D. Huang, J. S. Duker, and J. G. Fujimoto, "Swept source/Fourier domain polarization sensitive optical coherence tomography with a passive polarization delay unit," Opt. Express **20**(9), 10229–10241 (2012).
30. J. Holmes, S. Hattersley, N. Stone, F. Bazant-Hegemark, and H. Barr, "Multi-channel Fourier domain OCT system with superior lateral resolution for biomedical applications," Proc. SPIE **6847**, 68470O, 68470O-9 (2008).
31. V. Jayaraman, J. Jiang, H. Li, P. J. S. Heim, G. D. Cole, B. Potsaid, J. G. Fujimoto, and A. Cable, "OCT imaging up to 760 kHz axial scan rate using single-mode 1310nm MEMS-tunable VCSELs with >100nm tuning range," Conference on Lasers and Electro-Optics Technical Digest (CD), PDPB2 (2011).
32. M. P. Minneman, J. Ensher, M. Crawford, and D. Derickson, "All-semiconductor high-speed akinetic swept-source for OCT," Proc. SPIE **8311**, 831116, 831116-10 (2011).
33. D. C. Adler, W. Wieser, F. Trepanier, J. M. Schmitt, and R. A. Huber, "Extended coherence length Fourier domain mode locked lasers at 1310 nm," Opt. Express **19**(21), 20930–20939 (2011).
34. W. Wieser, T. Klein, D. C. Adler, F. Trépanier, C. M. Eigenwillig, S. Karpf, J. M. Schmitt, and R. Huber, "Extended coherence length megahertz FDML and its application for anterior segment imaging," Biomed. Opt. Express **3**(10), 2647–2657 (2012).
35. B. Potsaid, V. Jayaraman, J. G. Fujimoto, J. Jiang, P. J. S. Heim, and A. E. Cable, "MEMS tunable VCSEL light source for ultrahigh speed 60kHz - 1MHz axial scan rate and long range centimeter class OCT imaging," Proc. SPIE **8213**, 82130M, 82130M-8 (2012).
36. I. Grulkowski, J. J. Liu, B. Potsaid, V. Jayaraman, C. D. Lu, J. Jiang, A. E. Cable, J. S. Duker, and J. G. Fujimoto, "Retinal, anterior segment and full eye imaging using ultrahigh speed swept source OCT with vertical-cavity surface emitting lasers," Biomed. Opt. Express **3**(11), 2733–2751 (2012).
37. W. Choi, B. Potsaid, V. Jayaraman, B. Baumann, I. Grulkowski, J. J. Liu, C. D. Lu, A. E. Cable, D. Huang, J. S. Duker, and J. G. Fujimoto, "Phase-sensitive swept-source optical coherence tomography imaging of the human retina with a vertical cavity surface-emitting laser light source," Opt. Lett. **38**(3), 338–340 (2013).
38. I. Grulkowski, J. J. Liu, B. Potsaid, V. Jayaraman, J. Jiang, J. G. Fujimoto, and A. E. Cable, "High-precision, high-accuracy ultralong-range swept-source optical coherence tomography using vertical cavity surface emitting laser light source," Opt. Lett. **38**(5), 673–675 (2013).

#192229 - $15.00 USD Received 14 Jun 2013; revised 15 Jul 2013; accepted 31 Jul 2013; published 6 Aug 2013

39. T.-H. Tsai, B. Potsaid, Y. K. Tao, V. Jayaraman, J. Jiang, P. J. S. Heim, M. F. Kraus, C. Zhou, J. Hornegger, H. Mashimo, A. E. Cable, and J. G. Fujimoto, "Ultrahigh speed endoscopic optical coherence tomography using micromotor imaging catheter and VCSEL technology," Biomed. Opt. Express **4**(7), 1119–1132 (2013).
40. Y. Tao and R. A. Schulz, "Heart development in Drosophila," Semin. Cell Dev. Biol. **18**(1), 3–15 (2007).
41. A. Li, C. Zhou, J. Moore, P. Zhang, T. H. Tsai, H. C. Lee, D. M. Romano, M. L. McKee, D. A. Schoenfeld, M. J. Serra, K. Raygor, H. F. Cantiello, J. G. Fujimoto, and R. E. Tanzi, "Changes in the expression of the Alzheimer's disease-associated presenilin gene in drosophila heart leads to cardiac dysfunction," Curr. Alzheimer Res. **8**(3), 313–322 (2011).
42. A. Li, O. O. Ahsen, J. J. Liu, C. Du, M. L. McKee, Y. Yang, W. Wasco, C. H. Newton-Cheh, C. J. O'Donnell, J. G. Fujimoto, C. Zhou, and R. E. Tanzi, "Silencing of the Drosophila ortholog of SOX5 in heart leads to cardiac dysfunction as detected by optical coherence tomography," Hum. Mol. Genet. (2013), doi:10.1093/hmg/ddt1230.
43. N. J. Curtis, J. M. Ringo, and H. B. Dowse, "Morphology of the pupal heart, adult heart, and associated tissues in the fruit fly, Drosophila melanogaster," J. Morphol. **240**(3), 225–235 (1999).
44. J. A. Izatt, M. R. Hee, G. M. Owen, E. A. Swanson, and J. G. Fujimoto, "Optical Coherence Microscopy in Scattering Media," Opt. Lett. **19**(8), 590–592 (1994).
45. A. D. Aguirre, P. Hsiung, T. H. Ko, I. Hartl, and J. G. Fujimoto, "High-resolution optical coherence microscopy for high-speed, in vivo cellular imaging," Opt. Lett. **28**(21), 2064–2066 (2003).
46. C. Zhou, D. W. Cohen, Y. H. Wang, H. C. Lee, A. E. Mondelblatt, T. H. Tsai, A. D. Aguirre, J. G. Fujimoto, and J. L. Connolly, "Integrated optical coherence tomography and microscopy for ex vivo multiscale evaluation of human breast tissues," Cancer Res. **70**(24), 10071–10079 (2010).
47. C. Zhou, Y. H. Wang, A. D. Aguirre, T. H. Tsai, D. W. Cohen, J. L. Connolly, and J. G. Fujimoto, "Ex vivo imaging of human thyroid pathology using integrated optical coherence tomography and optical coherence microscopy," J. Biomed. Opt. **15**(1), 016001 (2010).
48. S. W. Huang, A. D. Aguirre, R. A. Huber, D. C. Adler, and J. G. Fujimoto, "Swept source optical coherence microscopy using a Fourier domain mode-locked laser," Opt. Express **15**(10), 6210–6217 (2007).
49. H. C. Lee, C. Zhou, D. W. Cohen, A. E. Mondelblatt, Y. H. Wang, A. D. Aguirre, D. J. Shen, Y. Sheikine, J. G. Fujimoto, and J. L. Connolly, "Integrated optical coherence tomography and optical coherence microscopy imaging of ex vivo human renal tissues," J. Urol. **187**(2), 691–699 (2012).

1. Introduction

High speed, high resolution and high sensitivity are desirable for optical coherence tomography (OCT), an emerging "optical biopsy" technique with resolutions approaching that of histopathology [1–3]. OCT imaging speed, characterized by the number of axial scans per second (A-scans/s), is limited by the line rate of line-scan cameras for spectral-domain OCT, or by the laser sweep rate for swept-source OCT, respectively. Commercially available line-scan cameras and tunable lasers operate at about 20,000 – 300,000 A-scans/s [4–6]. A number of approaches have been pursued to improve OCT imaging speed. The first approach is to develop high-speed line-scan cameras or high sweep rate tunable lasers. A record sweep rate of 5.2 MHz was demonstrated [7] using the Fourier-domain mode-locking (FDML) laser technology [8, 9]. However, as the axial scan rate increases, the dwell time at each imaging point decreases proportionally, resulting in a significant reduction in image sensitivity [10–12]. In general, the number of sampling points for each axial scan decreases as the axial scan rate increases. For tunable lasers, the wavelength sweep range is often compromised when the laser sweep rate increases, reducing the axial image resolution for OCT [7]. The second approach is to use parallel detection channels to improve OCT imaging speed [7, 13–16]. However, the scalability of this approach is poor due to unfavorable cost scaling. The high system complexity and the associated cost have prohibited wide utilization of multi-beam OCT systems using parallel detection channels to date.

Extended imaging range with minimal sensitivity roll-off can be highly beneficial for ranging applications and for imaging samples with large variation of surface topography, such as whole eye imaging, endoscopic and cardiovascular imaging. Several techniques have been developed to increase the axial imaging range of Fourier-domain OCT. These include phase shifting using a piezo translator [17] or an electro-optic phase modulator [18] on the reference arm, heterodyne detection [19, 20], polarization encoding [21], BM-mode scanning [22], dispersion encoding [23], coherence revival [24], and depth-multiplexing [25]. Depth-multiplexing techniques have also been utilized in simultaneous imaging of anterior segment and retina [26], and in polarization-sensitive OCT systems for simultaneously detection of orthogonal polarization states using electric-optic or acousto-optic devices [27] or passive optical delay units [28, 29]. A commercial OCT system, *i.e.* the VivoSight OCT scanner from

#192229 - $15.00 USD Received 14 Jun 2013; revised 15 Jul 2013; accepted 31 Jul 2013; published 6 Aug 2013

Michelson Diagnostics Ltd., utilizes multiple beams focused at different depths on samples to obtain extended depth of focus [30].

With the advancements in swept-source technology, there has been great interests in developing OCT light sources with extended coherence length for obtaining longer imaging range [13, 31–38]. Recently developed wavelength tunable vertical cavity surface-emitting lasers (VCSEL) achieved coherence length of over 50 mm [36, 38]. Due to high scattering in biological tissues and limited depth of focus in order to achieve micron-scale transverse resolutions, OCT imaging depth is generally within 1-2 mm from the tissue surface. This provides a unique opportunity to further increase OCT imaging speed by utilizing the long coherence length property of newly developed tunable lasers.

Here, we demonstrate a space-division multiplexing (SDM) technology that translates long coherence length of a commercially available tunable laser into high OCT imaging speed. We achieved an effective 800,000 A-scans/s imaging speed using a commercial 100,000 Hz tunable VCSEL light source [31, 35–39]. The SDM technology provides a new orthogonal dimension for further speed improvement for OCT with favorable cost scaling. The SDM-OCT technology we present here can achieve an order of magnitude or more improvement in imaging speed without compromising axial image resolution. SDM-OCT also allows synchronized cross-sectional and three-dimensional (3D) imaging of biological samples, enabling new biomedical applications.

2. Methods

2.1. Space-division multiplexing OCT system

Figure 1 demonstrates the concept for SDM-OCT. The key of the technology is to create multiple imaging beams to illuminate the sample simultaneously, while having different optical delays for each beam [see the red rectangular region in Fig. 1(a). For simplicity, only 4 beams are shown in the figure]. This was realized by using a planar lightwave circuit (PLC) splitter and a fiber array [Fig. 1(b)]. Returned signal from different sample locations were combined at the PLC splitter and interfered with light from the reference arm. A single detector and a high speed data acquisition card were utilized to record interference signal from all beams simultaneously. Since each beam was optically delayed, signal from different locations was presented at different frequency range [i.e. imaging depth, Fig. 1(c)]. Since all the beams were scanned together, synchronized imaging from multiple sample locations was enabled. This technique allows parallel imaging from multiple sample locations and therefore improves OCT axial scan rate by a factor equal to the number of beams used simultaneously.

A commercial VCSEL tunable laser (SL1310V1, Thorlabs Inc.) with a center wavelength of 1310 nm was used for the prototype SDM-OCT system. The laser has a sweep rate of 100,000 Hz, a duty cycle of ~65%, a tuning range of 100 nm, a coherence length of over 50 mm, and output power of 37 mW. A 95/5 optical coupler (AC Photonics, Inc.) was connected to the laser output. Five percent of the light was directed to a Mach-Zender interferometer (MZI), which had an optical path length difference of 60 mm in air. The remaining 95% of the light was used for OCT imaging. A 90/10 optical coupler provided 10% of the light to the reference arm and 90% of the light to the sample arm. Input light to the sample arm was split into 8 fibers using a PLC splitter (PLC Connections, LLC.). Output fibers from the PLC splitter were custom arranged in a one-dimensional (1D) array [1x8, Fig. 1(b)], with a length difference of 2.5 mm between each optical fiber. Spacing was ~300 μm between each fiber in the 1D array and ~370 μm after the spots were projected on samples. Surface of the fiber array was angle polished at 8 degree to minimize light reflection. An f = 30mm collimator was used in the sample arm, resulting in ~8 mm beam diameters. Light from different fibers were focused onto different spots on the sample, which were synchronously scanned by a pair of galvanometers (6215H with a pair of 10 mm mirrors, Cambridge Technology, Inc.). A 5X objective lens (Mitutoyo, 5X NIR) was utilized to provide ~11 μm transverse resolutions. Each spot had ~2 mW power on sample. Light intensity variation among all the spots was less than 1 dB. Optical circulators (AC Photonics, Inc.) were utilized on both the sample and

#192229 - $15.00 USD Received 14 Jun 2013; revised 15 Jul 2013; accepted 31 Jul 2013; published 6 Aug 2013

reference arms to route reflected signal from both arms to interfere at a 50/50 coupler. Broadband balanced detectors (1.6 GHz, PDB480C-AC, Thorlabs Inc.) were used to detect interference signal from both OCT and MZI systems. Outputs of the balanced detectors were digitally acquired simultaneously using a high speed data acquisition card (ATS9360, without on-board memory, Alazar Technologies Inc.) at 1.2 GS/s. Data from both channels (8320 points for each channel per sweep) was streamed to the computer memory continuously through a PCIe 8x port. The entire imaging range of the prototype system was about 35 mm in air.

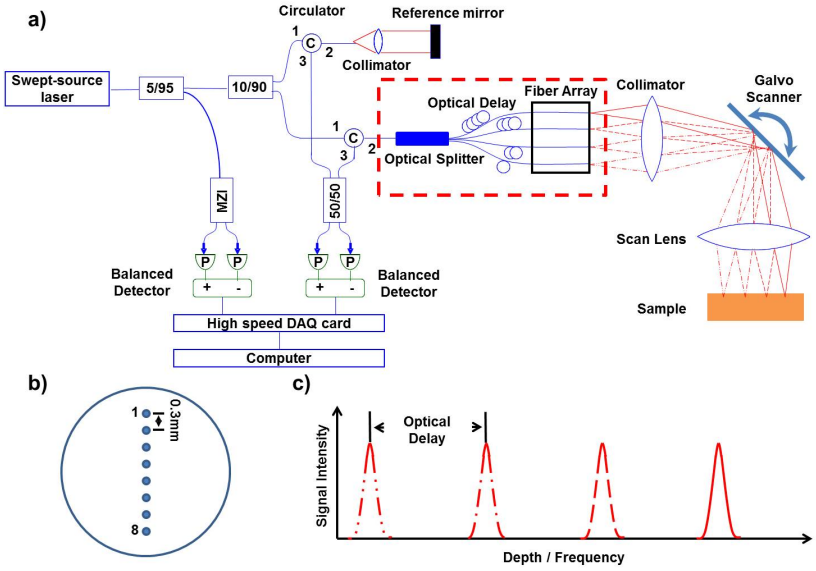

Fig. 1. Concept for SDM-OCT. **a).** Schematic diagram of the prototype SDM-OCT system. The key of the technology is to create multiple illumination beams on the sample simultaneously, while having different optical delays for each beam (see the red rectangular region). A single detection channel was used to collect signals from all beams simultaneously. **b).** A 1x8 fiber array with 300 μm spacing between individual fibers was used in the prototype system. **c).** Each beam was optically delayed. Signals from different beams (different sample locations) were presented at different frequency range (i.e. imaging depth). For simplicity, only 4 beams are shown.

2.2. Drosophila melanogaster larvae preparation

Drosophila melanogaster is a widely used model system for genetic and developmental biology studies due to the ease in culturing and its short lifecycles. *In vivo* SDM-OCT images were obtained from third instar *Drosophila* larvae. At this stage, the heart tube is located at the dorsal midline, spanning segments T2 (anterior end) to A8 (posterior end), being attached to its dorsal epidermis by seven pairs of alary muscles [40]. The larva was gently mounted onto a black clip board using a double-sided tape with its dorsal side facing upwards for imaging. No anesthesia was used to immobilize the *Drosophila* larvae.

2.3. In vivo *imaging and signal processing*

In order to image an entire *Drosophila* larva, all 8 beams in the SDM-OCT system were illuminated along the larva dorsal midline simultaneously. A 3D data set, consisting 400 x 80 laser sweeps with each beam scanned a 1.1 mm x 0.4 mm range, was acquired in 0.37 s. The MZI signal acquired simultaneously with the OCT signal was used for phase calibration of each laser sweep [36]. Images from the 8 beams were segmented from different depth range and digitally combined to form a volumetric data set consisting 400 x 605 A-scans covering the entire larva (1.1 mm x 3.0 mm range) using a custom written Matlab script. There were

#192229 - $15.00 USD Received 14 Jun 2013; revised 15 Jul 2013; accepted 31 Jul 2013; published 6 Aug 2013

about 5 B-scans overlapping for adjacent 3D volumes from the 8 beams. To obtain M-mode imaging from the larva heart, 400 B-scans with each containing 400 A-scans over 250 μm range around the heart tube were acquired in 2 s (~217 frames per second). Images from all 8 beams were collected simultaneously, although only images from three different heart segments were digitally combined and presented side-by-side for comparison. Functional information of the heart was analyzed following established methods [41, 42]. Matlab (Mathwork, Inc.) was used to process the data. ImageJ (NIH) and Amira (VSG, Inc.) were used to generate videos and render images for presentation.

3. Results

3.1. Point-spread-functions (PSFs) and sensitivity roll-off measurements

Figure 2 shows point-spread-functions (PSFs) and sensitivity roll-off measurements of the prototype system. A pin-hole was used on the sample arm to allow only the center beam to pass through for these measurements. A 94.6 dB sensitivity was measured using a calibrated reflector (–43.4 dB) and a sensitivity roll-off of < 2 dB was observed at ~30 mm imaging depth. The axial resolution was measured to be ~11 μm in air (or ~8.3 μm in tissue) throughout the entire depth range.

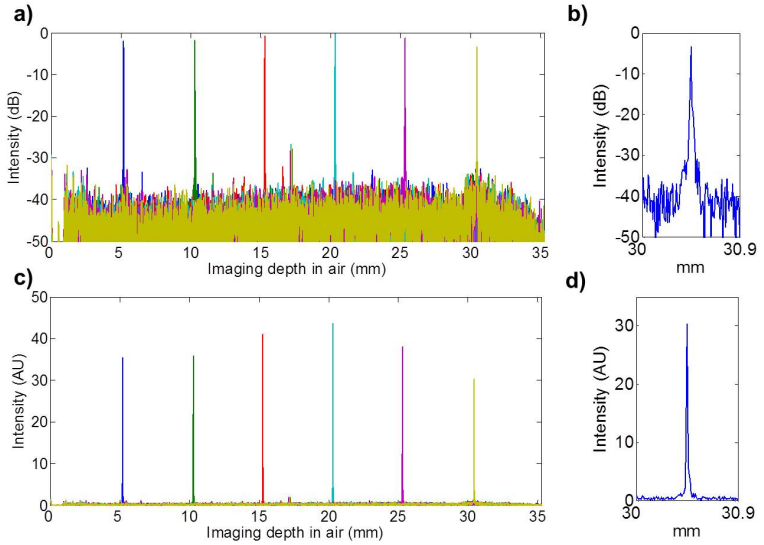

Fig. 2. Point spread functions (PSFs) and sensitivity roll-off measurements of the SDM-OCT imaging system. **a).** and **c).** Log and linear scale plot of the PSFs throughout the entire imaging depth. **b).** and **d).** Log and linear PSFs at ~30 mm imaging depth.

3.2. SDM-OCT imaging of Scotch tapes

We first performed SDM-OCT imaging on a roll of Scotch tape [Fig. 3] in order to demonstrate the image quality. As shown in Fig. 3(a), tape images seen from different depth corresponded to images obtained from different beams labeled as 1 to 8. Figure 3(b) shows magnified images of the tape at locations 1 through 8. Relatively uniform image intensity was observed from all the beams. Even at the deepest imaging depth (beam #8), layers of the tape were clearly visible. Since the laser was operated at 100,000 Hz, an effective 800,000 A-scans/s was achieved combining signals from all 8 beams.

#192229 - $15.00 USD Received 14 Jun 2013; revised 15 Jul 2013; accepted 31 Jul 2013; published 6 Aug 2013

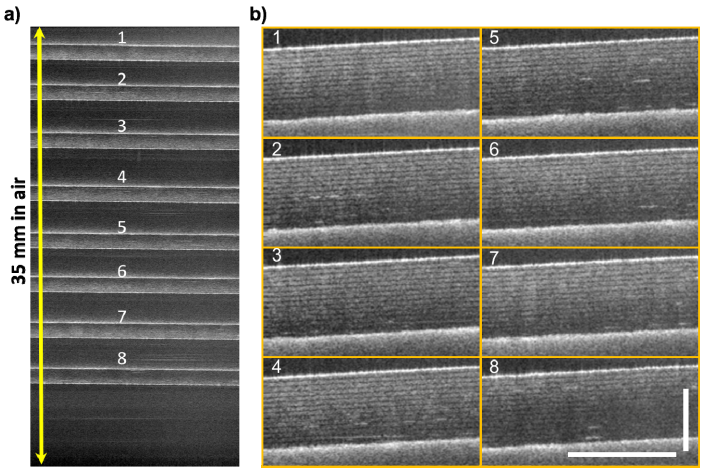

Fig. 3. SDM-OCT imaging of a roll of Scotch tape. **a).** Representative B-scan image of the tape. An imaging depth of 35 mm in air was obtained. Tape images seen from different depth (labeled as 1 to 8) corresponded to images obtained from different beams. **b).** Magnified view of tape images at locations 1 to 8. Layers of the tape were clearly visible even at the deepest imaging range (beam #8). An effective OCT imaging speed of 800,000 A-scans/s was achieved combining all 8 beams. Scale bars, 500 µm.

3.3. 3D SDM-OCT imaging of Drosophila larva

We further demonstrated *in vivo* 3D SDM-OCT imaging of a *Drosophila* larva [**Fig. 4**]. The entire 3D data set [400 x 605 A-scans, Fig. 4(a), and Media 1], assembled using images from all 8 beams, was acquired in 0.37 second. Figures 4(b) and 4(c) show cross-sectional and *en-face* images of the larva, respectively. The heart tube and the trachea structures were clearly observed.

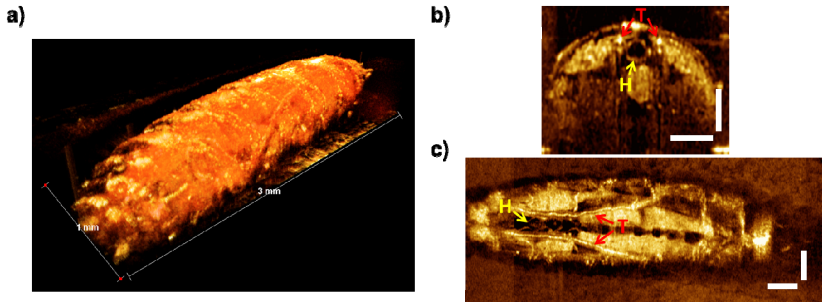

Fig. 4. *In-vivo* 3D SDM-OCT imaging of a *Drosophila melanogaster* larva. a). 3D volumetric data of a *Drosophila* larva (400 x 605 A-scans, Media 1) was obtained in 0.37 second by combining images from all 8 beams. **b).** Cross-sectional and c). *en-face* images of the larva, showing the heart tube and the trachea structures clearly. Scale bars, 250 µm.

3.4. Synchronized imaging of drosophila larva heart using SDM-OCT

To demonstrate synchronized imaging capability, we performed M-mode B-scan imaging (217 frames per second) over three segments of another larva heart, estimated to be the A7, A6, and A5 segments. A representative cross-sectional image showing three segments of the heart tube is shown in Fig. 5. A video demonstrating synchronized beating of the segments is provided as Media 2. We further quantified cardiac functions of the larva using a method we developed earlier [41, 42]. In addition to quantifying heart rate (372 beats per minute), end systolic (36 µm for A7, 32 µm for A6, and 11 µm for A5) and diastolic dimensions (60 µm for

#192229 - $15.00 USD Received 14 Jun 2013; revised 15 Jul 2013; accepted 31 Jul 2013; published 6 Aug 2013

A7, 74 μm for A6, and 58 μm for A5) and fractional shortening (42% for A7, 56% for A6, and 80% for A5), we also observed a delay between the dilation and contraction in segment A6 compared to A7 (14 ms), and segment A5 compared to A6 [69 ms, Fig. 6]. This delay suggested the contraction of the heart tube was initialized in the posterior segment and propagated toward the anterior segment. This finding is consistent with previous literatures on *Drosophila* larvae heart development [43].

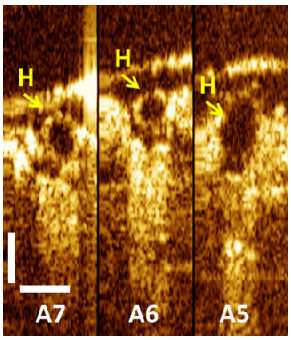

Fig. 5. Synchronized B-scan imaging over three segments (A7 – A5) of a larva heart (Media 2). Scale bars, 100 μm.

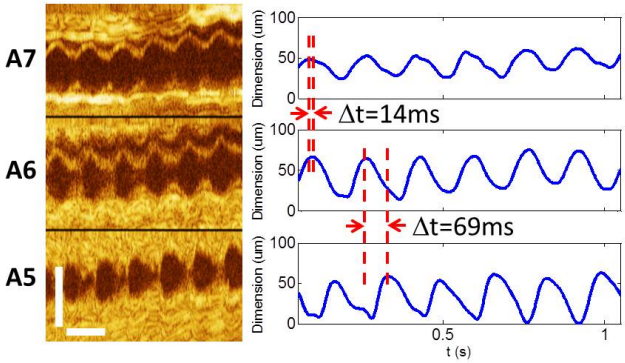

Fig. 6. M-mode images of the three heart segments (A7 – A5) and measurements of transverse heart chamber dimensions. Time delays between dilation and contraction in the three segments suggested that the contraction of the heart tube was initialized in the posterior segment and propagated toward the anterior segment. Scale bars, Vertical, 100 μm, horizontal, 0.2 s.

4. Discussions

The SDM technology provides a new orthogonal dimension to improve OCT imaging speed. It can be used in combination with ultrahigh speed tunable lasers with long coherence length, such as VCSEL [35, 38] and FDML [34] lasers, to achieve further speed improvement. Here, we demonstrated an 8x improvement in OCT imaging speed, although higher axial scan rate can be readily realized. In fact, with SDM-OCT, the axial scan rate is scalable to the number of beams used simultaneously. For optical coherence microscopy (OCM) applications [44–49], where the imaging penetration depth is limited to less than a few hundred microns, 16 channels or more can be easily implemented using current detection hardware. There is also flexibility in choosing the length difference between channels to accommodate variations in sample surface topography. Alternative arrangement of the fiber array (*e.g.* 2D) can also be utilized for different applications.

Fundamentally, SDM-OCT may have resolution and sensitivity advantages compared to single-spot OCT with increased laser sweep rate or camera line rate. In our demonstration, the axial resolution was not compromised when we obtained 8x higher axial scan rate, since the

#192229 - $15.00 USD Received 14 Jun 2013; revised 15 Jul 2013; accepted 31 Jul 2013; published 6 Aug 2013

laser tunable range was not changed. Meanwhile, the dwell time at each imaging spot was longer using a low tunable rate laser. More photons were reflected from the sample and more data sampling points were recorded within the dwell time for SDM-OCT. This was in contrast to the standard approach, where the dwell time and the number of sampling points for each axial scan were reduced in order to achieve high axial scan rate. For example, assuming the same power level at the imaging spot, a single-spot system running at 800 kHz would have 8 times less photons reflected back from the sample within the dwell time, compared to an 8 x 100 kHz SDM-OCT system. This corresponds to ~9 dB sensitivity reduction for the single-spot OCT system. In our current prototype system, however, the PLC splitter had a ~10 dB insertion loss. This was not an issue in the forward direction, where the input light was evenly split into the 8 beams. However, when combining reflected light from the sample, the 10 dB insertion loss resulted in a significant reduction in sensitivity. As a result, we achieved only ~95 dB sensitivity over the entire imaging range when ~2 mW light was shine on the sample at each imaging spot. This was about 11 dB lower compared to the shot-noise-limited sensitivity. In the future, alternative designs bypassing the PLC splitter in the return path may be utilized to further improve imaging sensitivity.

With the SDM technology, the bottleneck for further improving swept-source OCT imaging speed is no longer the sweep rate of tunable lasers. Instead, high speed data acquisition and high throughput data transfer are greatly desired. The data acquisition card in our prototype system supports a 12-bit 1.8 GS/s sampling rate. However, due to limited data transfer rate, we could only sample the OCT and MZI channels simultaneously at 1.2 GS/s. Further improvement in data acquisition and transfer rate, bandwidth of the detectors, coherence length of the light source, and number of fiber channels will further scale up OCT axial scan rate linearly with minimum additional cost. Since the input light is split into multiple beams, a powerful light source is also desirable.

5. Conclusions

In summary, we demonstrated a space-division multiplexing technique for OCT. SDM-OCT achieves significant improvement in axial scan rate and preserves axial imaging resolutions using a passive optical component and a single detection channel. This technique enables synchronized cross-sectional and 3D imaging of biological samples, and provides a new cost favorable approach to further improve OCT axial scan rate. SDM-OCT may be applied to a wide range of structural and functional OCT applications, including but not limited to ophthalmology, cardiovascular imaging, endoscopic imaging, cancer imaging and dental applications.

Acknowledgments

The authors thank Thorlabs Inc., especially Anjul Davis and James Jiang, for providing early access to the first commercially available VCSEL laser, Airong Li for providing Drosophila melanogaster samples, Desmond Adler, Tony Ko, James Jiang, Joel H. Greenberg and Arjun G. Yodh for providing constructive feedbacks. This work was supported by Lehigh University Start-up Fund, and the National Institute of Health / National Institute of Biomedical Imaging and Bioengineering (NIH/NIBIB) Pathway to Independence Award (R00-EB010071 to C.Z.).

#192229 - $15.00 USD Received 14 Jun 2013; revised 15 Jul 2013; accepted 31 Jul 2013; published 6 Aug 2013